(Received 6 March 2026, Accepted 17 April 2026, Scheduled 3 June 2026)

A Miniaturized Long-Read-Range Anti-Metal UHF RFID Tag Antenna for Full-Process Management of Bank Cash Transport Boxes

Bingqing Yao*

Anhui Institute of International Business, Hefei 231131, China

ABSTRACT: In this study, a miniaturized long-read-range anti-metal Ultra-high frequency (UHF) RFID tag patch antenna for bank cash transport boxes is presented. Short-circuit inductors were loaded on the side of the antenna, and double H-shaped slots were etched on the patch surface. These structures extend the current path and increase the electrical length, which lowers the resonant frequency and enables antenna miniaturization. The antenna impedance can be flexibly tuned by adjusting the position and width of the short-circuit inductors and the length of the double H-shaped slots. Conjugate matching with the RFID chip is therefore achieved to ensure maximum power transfer. In addition, the short-circuit inductors reduce the influence of the metal plate and improve the current distribution. Consequently, the radiation efficiency is enhanced, and a long reading distance is obtained. The proposed antenna was fabricated and measured, and good agreement between the simulation and measurement results was observed. The measured results show that the antenna occupied an area of 615 mm^2 and achieved a maximum reading distance of 12.4 m when mounted on a metal cash-in-transit box. The presented antenna is suitable for full-process management of bank cash transport boxes in different application scenarios.

1. INTRODUCTION

Intelligent systems are a primary trend in next-generation banking services. The full-process security management of cash-in-transit (CIT) boxes in cash allocation, transport, and storage has become increasingly important. Ultra-high frequency (UHF) RFID technology offers advantages such as contactless identification, long read range, and multi-tag recognition, making it an effective tool for automated management of cash-in-transit boxes. However, CIT boxes are often made of metal and impose strict requirements on tag size. Conventional UHF RFID tags are easily affected by image currents when placed on metal surfaces, resulting in degraded impedance matching, reduced radiation efficiency, and a significantly shortened read range [1–3]. Therefore, developing a UHF RFID tag antenna with strong anti-metal capability is of significant practical importance for the bank.

In recent years, various design methods have been proposed to address the impedance matching of anti-metal UHF RFID tag antennas. In [4], conjugate matching with the chip is achieved by adjusting coupled arc-shaped open stubs. In [5], a dual T-type matching structure and multiple open stubs are used to tune the impedance, whereas a cylindrical ground plane reduces the influence of the metal. In [6], distributed inductors formed by bent inductive lines are employed to compensate for the the chip's high capacitance. However, these impedance-matching structures typically occupy a large area, which is undesirable for antenna miniaturization.

Several techniques have been proposed to reduce the size of tag antennas. In [7], shorting pins are used to construct a three-dimensional current path, thereby increasing the electrical length. In [8], shorting patches are introduced in the planar inverted-L antenna (PILA) structure to form a dual-layer inverted L antenna. In [9], I-shaped slots are loaded to extend the surface current path. Although these methods can effectively reduce antenna size, it is difficult to maintain a long-read range on metal surfaces. Therefore, achieving a high-performance anti-metal tag antenna that combines a compact size and long read range remains a significant challenge.

This paper proposes a miniaturized UHF RFID tag antenna with a long reading distance for bank cash-in-transit box applications. Short-circuit inductance and dual H-shaped slot structures were introduced into the antenna structure to extend the surface current path and increase the equivalent electrical length, thereby achieving antenna miniaturization. Conjugate matching between the antenna and RFID chip was realized by adjusting the position of the shorting inductor and the length of the dual H-shaped slot, allowing a relatively long read distance to be exhibited on metal surfaces and providing good anti-metal performance. Finally, a prototype of the proposed tag antenna is fabricated and experimentally evaluated. The simulated and measured results are in good agreement, validating the effectiveness of the proposed design.

2. ANTENNA STRUCTURE AND DESIGN

The structure of the proposed RFID tag antenna is illustrated in Fig. 1. The main radiating element is a circular patch, with

* Corresponding author: Bingqing Yao (392160435@qq.com).

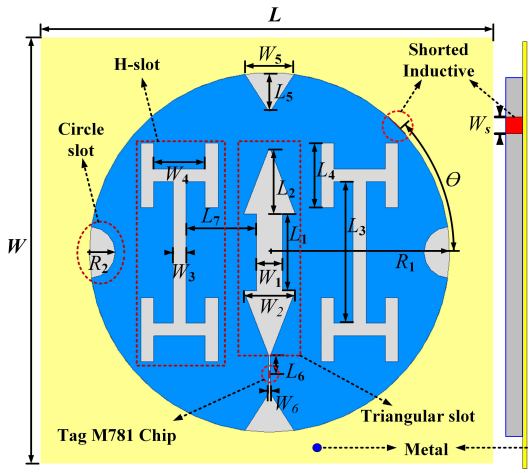

FIGURE 1. Geometry of the proposed RFID tag antenna.

two triangular slots etched along the axial direction to form a closed-loop current path. To achieve antenna miniaturization, a shorting inductor is loaded at the side of the antenna, and a semicircular slot together with a dual H-shaped slot is etched on the patch surface. These structures effectively extend the surface current path, increase the electrical length, and consequently reduce the resonant frequency.

By adjusting the position of the shorting inductor and the length of the dual H-shaped slot, the antenna impedance can be flexibly tuned to realize conjugate matching with the tag chip, thereby ensuring maximum power transfer. In addition, the introduction of the shorting inductor alleviates the influence of the metal plate on the antenna and optimizes the current distribution, which further enhances the radiation efficiency and enables a longer reading distance.

The Impinj M781 chip is adopted as the RFID tag chip in this design, exhibiting an input impedance of $10 - j167\,\Omega$ at the operating frequency of 915 MHz.

As shown in Fig. 2, the equivalent circuit model of the proposed tag antenna is presented, which can be used to analyze the input impedance and assist in antenna design. The tag antenna is divided into several sections, and the corresponding equivalent element values are derived. The main radiating structure consists of two semicircular patches that are symmetrically arranged, and each can be represented by a parallel RLC resonant circuit. In this model, the total resistance of the patch is $R_p = R_{rad} + R_{loss}$, which can be calculated as [9]:

$$R_{rad} = \frac{h^2}{8\pi f_r \varepsilon_0 w_p L_e} \tag{1}$$

where h is the substrate thickness, f_r is the center frequency of 915 MHz, L_e represents the fringing-field extension length, w_p denotes the equivalent width of the patch.

$$R_{loss} = \frac{(l_p/2)\,\rho K_c}{w_p t\left\{1 - \exp\left[-\frac{2\sigma}{t}\left(1 + \frac{t}{w_p}\right)\right]\right\}} \tag{2}$$

where σ is the skin depth, t is the copper thickness, ρ is the copper resistivity, K_c is the current spreading factor, l_p denotes the equivalent length and width of the patch.

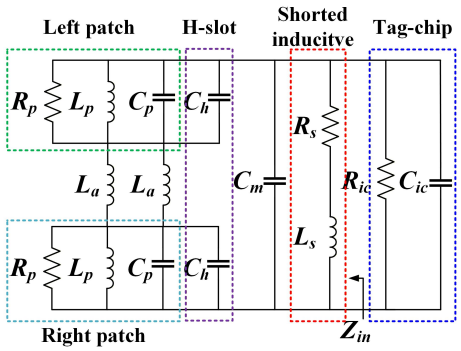

FIGURE 2. Equivalent circuit model of the proposed tag antenna ($R_p = 2683\,\Omega$, $L_p = 7.11\,\text{nH}$, $C_p = 6.69\,\text{pF}$, $C_h = 0.487\,\text{pF}$, $L_a = 1.48\,\text{nH}$, $C_m = 1\,\text{pF}$, $R_s = 0.0\,\Omega$, $L_s = 8.52\,\text{nH}$, $R_{ic} = 2.8\,\Omega$, $C_{ic} = 1.04\,\text{pF}$).

Owing to the electric field effect, the space between the radiating patch and the ground plane can be modeled as a pair of parallel capacitor plates, which is equivalently represented by the total patch capacitance C_p. The loaded inductance L_p of the patch can be calculated as follows [10]:

$$C_p = \frac{\varepsilon_0 \varepsilon_r A_e}{h} \tag{3}$$

$$L_p = 200\,(l_p/2)\left[\ln\left(\frac{2l_p}{w_p + t}\right) + 0.50049 + \frac{w_p + t}{3\,(l_p/2)}\right] \tag{4}$$

where A_e represents the effective surface area.

Moreover, the resistance of the shorting stub is $R_s = 2[(\rho l_s)/(w_s t)][K_c/(1 - e^{-x})$, where l_s and w_s are the length and width of the shorting stub, respectively, and $x = 2(1 + t/w_s)(\sigma t)$. The inductance of the shorting stub is $L_s = 400 l_s\{\ln[2l_s/(w_s + t)] + 0.50049 + [(w_s + t)/3l_s]\}$ [11]. R_{ic} and C_{ic} denote the resistance and load capacitance of the tag chip, respectively. To achieve maximum power transfer, the input impedance Z_{in} of the tag antenna should be designed as $10 + j167\,\Omega$, which is the complex conjugate of the chip impedance.

Based on the above analysis, all calculated parameter values are added to the legend in Fig. 2. In addition, the input impedance Z_{in} of the proposed tag antenna can be employed to assist the antenna design and can also be expressed in terms of the input admittance Y_{in}.

$$Y_{in} = \frac{1}{R_s} + \frac{1}{j\omega L_s} + j\omega C_m + 2\left[\frac{1}{R_p} + \frac{1}{j\omega L_p} + j\omega\,(C_p + C_h) + \frac{1}{j\omega L_a}\right] \tag{5}$$

As shown in Fig. 3(a), the initial structure is a circular patch antenna with two triangular slots etched along the axial direction to form a closed-loop current path. Under this condition, the current density is mainly concentrated at the center of the patch. As illustrated in Fig. 4, the initial structure resonates at 1.306 GHz, which is significantly higher than the target center frequency of 915 MHz. The corresponding input impedance

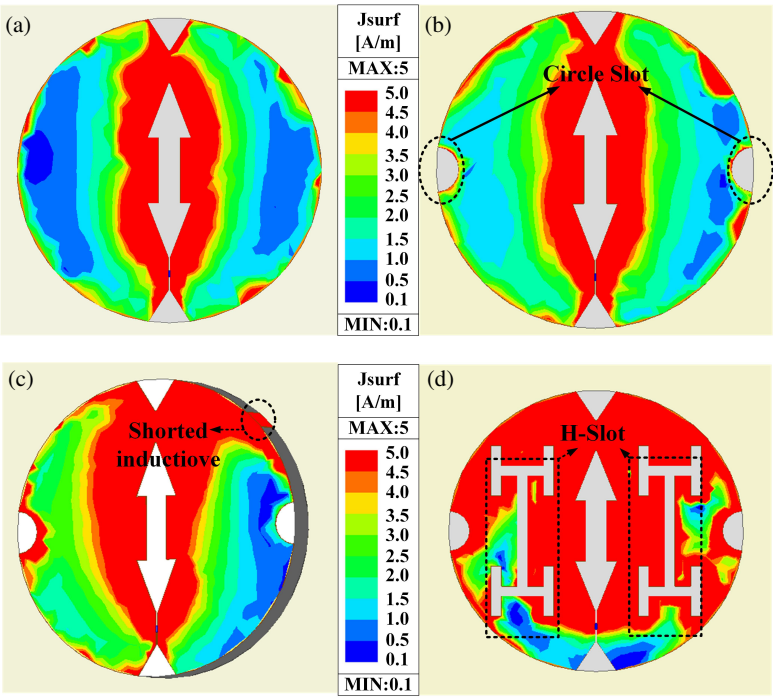

FIGURE 3. Current distributions of loading different structures. (a) Initial structure. (b) Circle slot. (c) Shorted inductive. (d) H-slot.

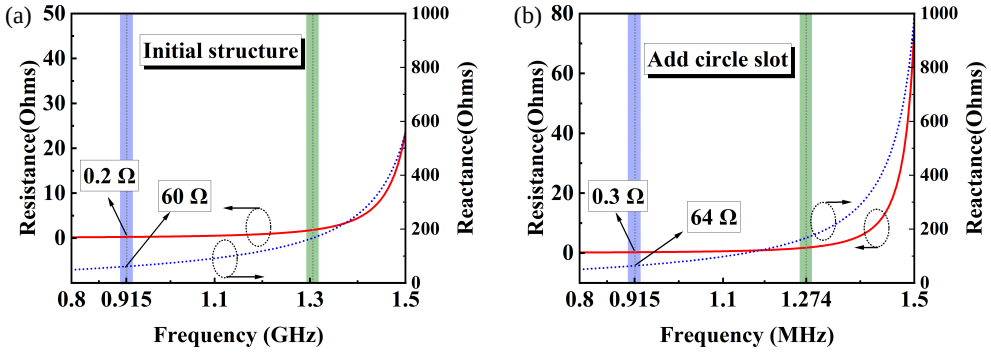

FIGURE 4. Comparison of input impedance for (a) initial structure, (b) circle slot.

is $0.2 + j60\,\Omega$, which does not satisfy the required conjugate matching condition of $10 + j167\,\Omega$.

To regulate the surface current distribution and extend the current path toward the patch edges, circular slots were further etched on both sides of the antenna. As shown in Fig. 3(b), after introducing the circular slots, the edge current cannot directly cross the slot region and is forced to flow around the slot periphery, thereby increasing the effective electrical length and reducing the resonant frequency. As depicted in Fig. 4, the resonant frequency decreased to 1.274 GHz after loading the semicircular slots, with an input impedance of $0.3 + j64\,\Omega$. Although an improvement was achieved, the resonant frequency remained higher than the design target.

To effectively shift the resonant frequency toward the UHF band, a shorting inductor with a width of 2 mm is introduced on the right side of the patch to establish an additional inductive loading path between the radiating patch and the ground plane. As shown in Fig. 3(c), after incorporating the shorting inductor, the surface current distribution is significantly redistributed from being centrally concentrated to spreading along the patch periphery, whereas the current density in regions away from the feeding side is notably enhanced. This behavior indicates that the shorting inductor forms an effective inductive coupling path between the radiator and the ground, thereby elongating the dominant current loop and increasing the equivalent electrical length, which leads to antenna miniaturization.

As illustrated in Figs. 5(a) and 5(b), the resonant frequency is further reduced to 956 MHz after loading the shorting inductor, which has an input impedance of $2 + j98\,\Omega$. Moreover, in the presence of a metallic backing plate, strong image currents are induced on the metal surface by the patch current, which distorts the near-field distribution and degrades the radiation performance. The introduced shorting inductor provides a low-impedance return path between the radiator and the ground [10].

To further reduce the resonant frequency while achieving miniaturization and impedance matching, dual H-shaped slots

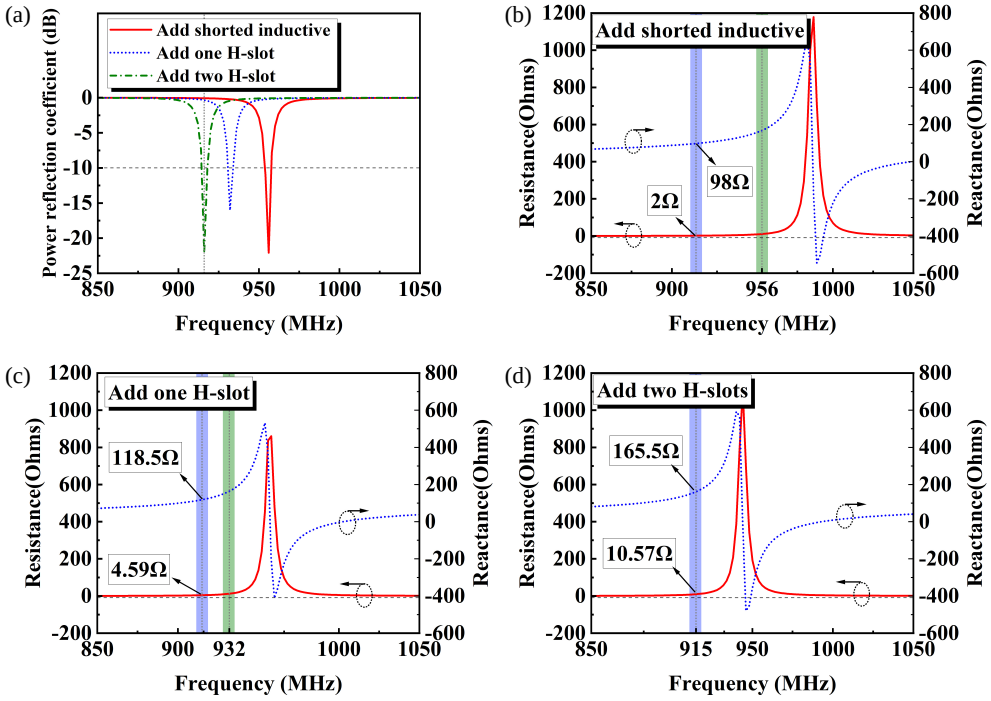

FIGURE 5. Comparison for loading different structures. (a) Power reflection coefficient. (b) Shorted inductive. (c) One H-slot. (d) Two H-slots.

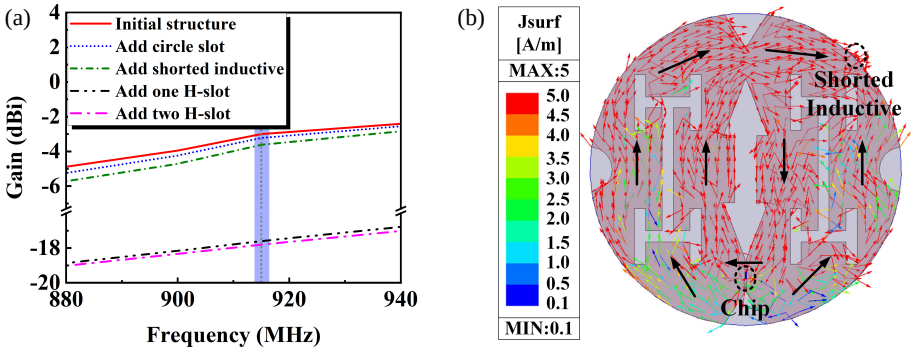

FIGURE 6. (a) Comparison of antenna gains for different structures. (b) Vector surface current distribution of the tag antenna.

are symmetrically etched on both sides of the patch. As shown in Fig. 3(d), after introducing the H-shaped slots, the surface current distribution expands markedly from the upper region toward the lower part of the patch, indicating a significant increase in the current flow region. This behavior demonstrates that the dual H-shaped slots introduce a longer meandering current path within the radiator, thereby increasing the equivalent electrical length and enabling antenna miniaturization.

As illustrated in Figs. 5(c) and 5(d), after loading a single H-shaped slot, the resonant frequency decreased to 932 MHz with an input impedance of $4.58 + j118.5\,\Omega$, which is slightly higher than the target center frequency of 915 MHz. To further optimize the performance, a second H-shaped slot was introduced, resulting in a resonant frequency of 915 MHz and an input impedance of $10.57 + j165.5\,\Omega$. These values are well conjugate-matched to the chip impedance of $10 - j167\,\Omega$. The results confirm that effective conjugate matching between the antenna and the tag chip was achieved, thereby ensuring maximum power transfer.

The realized gain of antennas with different structures is presented in Fig. 6(a). The realized gain of both the initial structure and the structure loaded with a circular slot is below -17 dBi. This is mainly attributed to poor impedance matching that causes the resonant frequency to deviate from the 915 MHz. After integrating a shorting inductor and the dual H-shaped slots, the realized gains are -3.62 dBi and -3 dBi, respectively. The short-circuited inductor mitigates the impact of the backing metal on the tag, while the dual H-shaped slots optimize the surface current distribution, thereby enhancing the radiation efficiency. Ultimately, the antenna achieves good conjugate matching with the chip and an improvement in the realized gain.

In addition, the vector surface current distribution of the final antenna structure is presented in Fig. 6(b). The current flows from the tag chip to the left side of the patch, then to the right, and finally returns to the chip, forming a closed loop. The dual H-shaped slots split the main loop current into two distinct paths, with current density concentrated at the edges of the

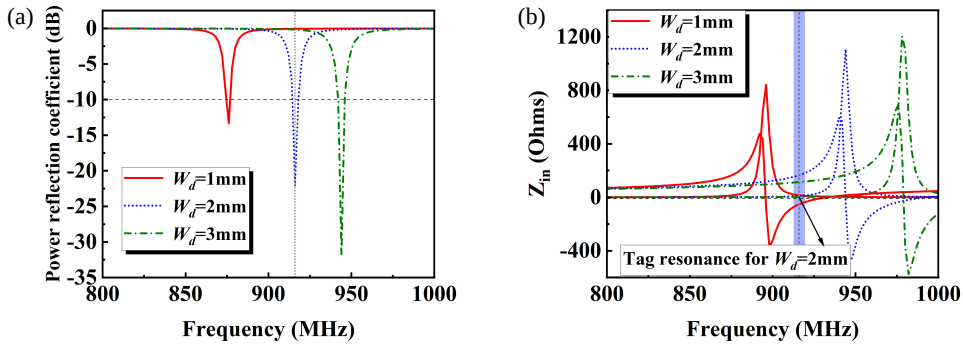

FIGURE 7. Effects of varying the width W_d of the shorted inductor on (a) power reflection coefficient, (b) input impedance.

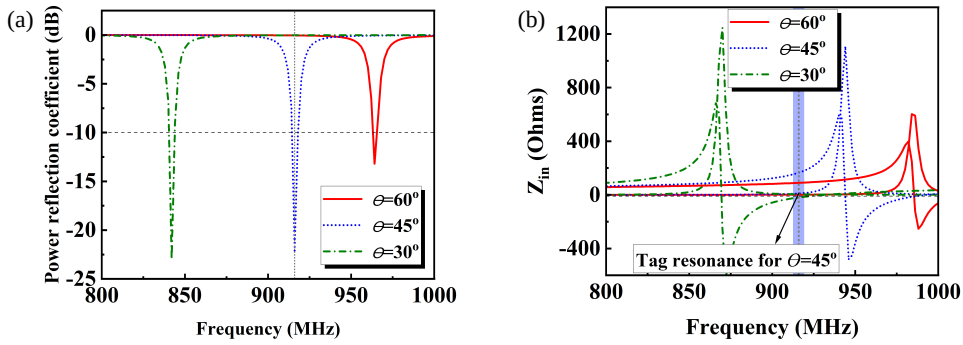

FIGURE 8. Effects of varying the position of the shorted inductor on (a) power reflection coefficient, (b) input impedance.

slots, which verifies their capability to adjust the resonant frequency of the antenna. The introduction of a short-circuited inductor induces a branch in the main loop current, creating a new path from the patch through the inductor to the ground. This mechanism extends the effective current path, leading to antenna miniaturization. Meanwhile, the majority of the current is concentrated near the short-circuited inductor, demonstrating its effectiveness in tuning the antenna's input impedance.

First, the effect of the shorting inductor width on the reflection coefficient and input impedance is shown in Fig. 7. From the figure, as the width W_d decreases, the input impedance of the antenna increases, while the resonant frequency decreases from 944 MHz to 876 MHz. This is due to the reduction in the width of the short-circuit inductance, which increases its equivalent inductance L_s, thereby lowering the resonant frequency.

Furthermore, the influences of the shorting inductor position on the reflection coefficient and input impedance are illustrated in Fig. 8. The position is characterized by the angle θ, when θ is 0°, the shorting inductor is located at the center of the right edge of the antenna. When θ is $-90°$, the shorting inductor is positioned at the feed point. As the θ value increases, the shorted inductor moves away from the feed point, the input impedance is decreased gradually, while the resonant frequency shifts from 964 MHz to 842 MHz.

This because the shorting inductor is placed closer to the high-density area, resulting in an increased effective inductive reactance, thereby lowering the resonant frequency [12]. Therefore, by jointly tuning the width and position of the shorting inductor, flexible control of the antenna resonant frequency can be achieved, which is beneficial for antenna miniaturization

3. MEASUREMENTS AND VERIFICATION

A prototype was fabricated to validate the performance, and the final parameters were optimized via full-wave simulation (HFSS). The specific values are determined as follows (mm): $R_1 = 14$, $R_2 = 13$, $R_3 = 14$, $P_1 = 1$, $P_2 = 8$, $P_3 = 21$, $P_4 = 3.4$, $P_5 = 18$, $W_1 = 0.4$, $W_2 = 2$, $W_3 = 5$, $\theta_1 = 7.5°$, $\theta_2 = 15°$. As shown in Fig. 9, the proposed tag antenna prototype with an overall size of 615 mm^2 × 2.5 mm was etched on a 0.035-mm-thick copper layer and fabricated on a circular Rogers 4350 substrate ($\varepsilon_r = 3.66$, $\tan\delta = 0.004$, radius = 14 mm, thickness = 2.5 mm), and measured at the center of a 250 mm × 250 mm × 1 mm metal plate to emulate the metallic backing effect.

As shown in Fig. 10, the vector network analyzer Keysight N5244 is employed to measure the input impedance of the tag antenna. A dual-port cable is connected to a dedicated test fixture via SMA connectors. The test fixture is attached to both sides of the gap at the tag chip's solder joint, enabling the extraction of the tag's S-parameters, and then the input impedance is calculated using the following formula [13]:

$$Z_{in} = \frac{2Z_0\left(1 - S_{11}^2 + S_{21}^2 - 2S_{21}^2\right)}{\left(1 - S_{11}\right)^2 - S_{21}^2} \tag{6}$$

where $Z_0 = 50\,\Omega$ is the characteristic impedance.

A comparison of the input impedance obtained from different models is shown in Fig. 11. It can be observed that the simulated antenna resonates at 915 MHz with an input impedance of $10.57 + j165.5\,\Omega$. In the measurement, the antenna resonated at 922 MHz with an input impedance of $10.7 + j165\,\Omega$,

TABLE 1. Comparisons with some of the previous tag antennas.

	EIRP (W)	P_{th} (dBm)	Tag volume (mm^3)	Metal size (mm^2)	Meas. RD (m)	NRD (m)
[2]	4	−20.85	3694	200 × 200	8.1	11
[3]	4	−17.3	3534	300 × 400	11.7	23.4
[4]	4	−20.85	8250	200 × 200	9	12.21
[5]	4	−18	3584	200 × 200	7.5	14.1
[6]	4	−17.8	3175.2	200 × 200	7.25	13.97
[7]	4	−20.85	2560	240 × 240	7.3	9.9
TW	**4**	**−23.5**	**1539**	**250 × 250**	**12.4**	

P_{th}: Chip sensitivity Meas. RD: Measured reading distance. NRD: Normalized reading distance.

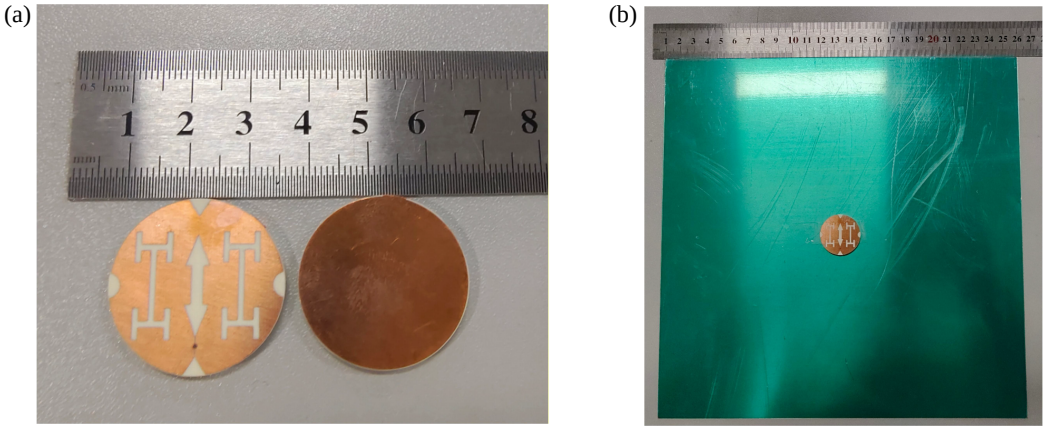

FIGURE 9. (a) Prototype of the RFID tag. (b) The tag is placed on the metal.

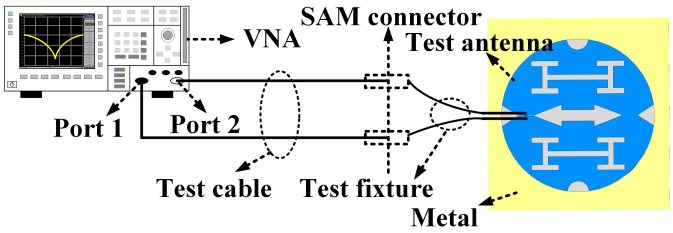

FIGURE 10. Schematic diagram of testing an antenna using the VNA.

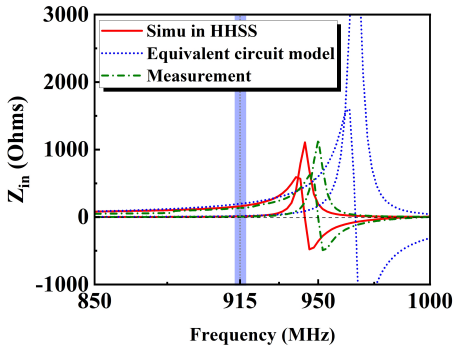

FIGURE 11. Comparison of input impedance between simulation and measurement results.

whereas the equivalent circuit model predicted a resonant frequency of 906 MHz with an input impedance of $11.9 + j167\,\Omega$. The input impedances obtained from all three approaches are well conjugate-matched to the chip impedance ($10 - j167\,\Omega$), thereby ensuring maximum power transfer. In addition, there is a difference between the equivalent circuit model and the simulation results. In the antenna structure, the parasitic capacitance generated by the triangular slot and double H-shaped slot cannot be accurately calculated through formulas to obtain equivalent parameter values. The equivalent circuit model cannot fully account for the coupling between units and edge field effects. However, the presented equivalent circuit model can still effectively predict the variation trend of impedance, providing reliable guidance for the design and optimization of the antenna.

As shown in Fig. 12(a), the reading distance was measured in a microwave anechoic chamber using a circularly polarized handheld reader (UROVO-DT50U) with an effective isotropic radiated power (EIRP) of 4 W. The tag, which was equipped with an M781 chip, was mounted at the center of the cash-in-transit box with its radiating surface parallel to the ground. During the entire measurement process, the reader was fixed on a movable fixture, and its radiating surface was maintained paral-

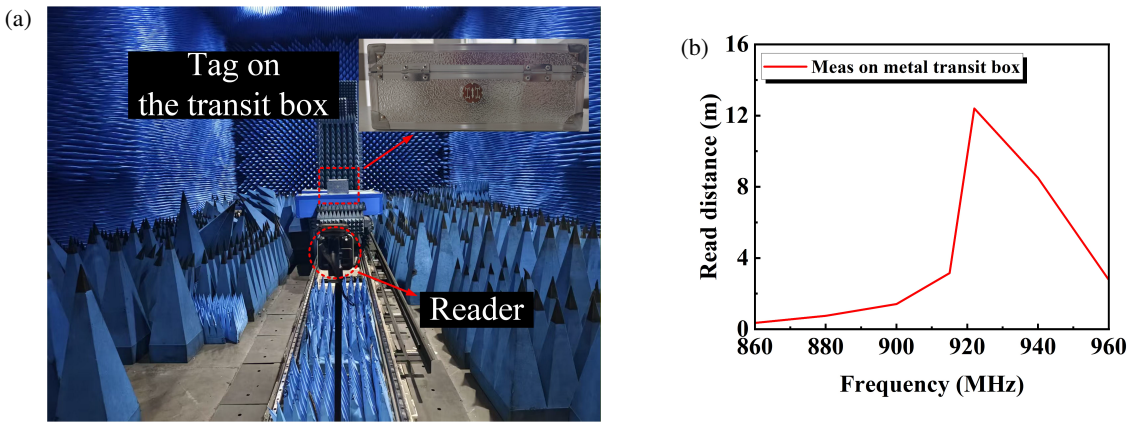

FIGURE 12. (a) Schematic diagram of testing the reading distance. (b) Measurement of reading distance.

lel to that of the tag. The fixture is moved gradually away from the tag under test until the tag can no longer be read, thereby determining the maximum reading distance. As illustrated in Fig. 12(b), the maximum measured reading distance on a metal cash-in-transit box is 12.4 m. Therefore, the proposed tag maintains a long reading range on metal surfaces, demonstrating that the proposed tag antenna is insensitive to the backing metallic platform and is well-suited for the identification of bank cash-in-transit boxes.

Finally, in Table 1, the performances of the proposed tag antenna are compared with previously reported designs when deployed on metallic platforms. For a fair comparison, the reading distance is normalized using the EIRP of 4W and the tag sensitivity P_{th} of -23.5 dBm of the proposed tag antenna, which can account for the effects of different EIRPs and tag sensitivities.

As shown in the table, the proposed tag achieves a compact size while maintaining a relatively long reading range in metallic environments compared with existing designs. Moreover, the proposed tag did not require a multilayer structure, thereby avoiding additional design and fabrication complexity. Overall, the proposed tag antenna demonstrated excellent anti-metal performance.

4. CONCLUSION

In this study, a miniaturized UHF RFID patch tag antenna with a long reading range is presented. Shorting inductor and dual H-shaped slots were introduced to effectively extend the surface current path and increase the equivalent electrical length, thereby reducing the resonant frequency and enabling antenna miniaturization. Measurement results demonstrated that the proposed antenna achieved a maximum reading distance of 12.4 m when mounted on a metal cash-in-transit box. Moreover, the tag antenna featured a compact structure, single-layer implementation, and ease of fabrication, making it suitable for full-process management of bank cash-in-transit boxes.

REFERENCES

[1] Ng, G.-J., E.-H. Lim, P.-S. Chee, and M. Murugesh, "Design of dual-band UHF RFID tag antenna using even and odd modes of asymmetric split ring for anti-metal applications," *IEEE Transactions on Antennas and Propagation*, Vol. 73, No. 1, 64–73, Jan. 2025.

[2] Huang, W., S. Hou, J. Hu, and P. Wang, "A broadband RFID tag antenna for metal surface with characteristic mode analysis," *IEEE Antennas and Wireless Propagation Letters*, Vol. 24, No. 6, 1427–1431, Jun. 2025.

[3] Lee, S.-R., W.-H. Ng, E.-H. Lim, and S. K. A. Rahim, "Loop-coupled small antenna with enhanced bandwidth for on-metal UHF RFID tag design," *IEEE Transactions on Antennas and Propagation*, Vol. 71, No. 4, 3660–3664, Apr. 2023.

[4] Erman, F., S. Koziel, E.-H. Lim, L. Leifsson, E. Hanafi, and M. Murugesh, "A low-profile metal-backed dipole loaded with closely coupled arc-shaped open stubs for on-metal tag design with wide frequency tuning capability," *IEEE Transactions on Antennas and Propagation*, Vol. 72, No. 4, 3772–3777, Apr. 2024.

[5] Wu, C., J. Yuan, and Z. Chen, "A UHF RFID tag antenna placeable on a metal surface without degraded performances," *IEEE Antennas and Wireless Propagation Letters*, Vol. 23, No. 7, 2101–2105, 2024.

[6] Murugesh, M., E.-H. Lim, P.-S. Chee, Y.-H. Lee, and F.-L. Bong, "Compact ring antennas with high-impedance line loaded with distributed inductors for on-metal tag design," *IEEE Transactions on Antennas and Propagation*, Vol. 70, No. 3, 1740–1749, Mar. 2022.

[7] Nguyen, M.-T., Y.-F. Lin, C.-H. Chen, Y.-C. Tseng, and H.-M. Chen, "Miniature 3-D-dipole antenna for UHF RFID tag mounted on conductive materials," *IEEE Transactions on Antennas and Propagation*, Vol. 70, No. 12, 11 454–11 464, Dec. 2022.

[8] Ooi, S.-Y., P.-S. Chee, E.-H. Lim, Y.-H. Lee, and F.-L. Bong, "Stacked planar inverted-L antenna with enhanced capacitance for compact tag design," *IEEE Transactions on Antennas and Propagation*, Vol. 70, No. 3, 1816–1823, Mar. 2022.

[9] Ng, G.-J., M. Murugesh, E.-H. Lim, P.-S. Chee, J.-H. Low, and C.-H. Tan, "Single-layer truncated patch antenna with an inclined I-slit for anti-metal tag design," *IEEE Journal of Radio Frequency Identification*, Vol. 8, 847–856, 2024.

[10] Chiang, S.-M., E.-H. Lim, P.-S. Chee, Y.-H. Lee, and F.-L. Bong, "Dipolar tag antenna with a top-loading inductive channel with

broad range frequency tuning capability," *IEEE Transactions on Antennas and Propagation*, Vol. 70, No. 3, 1653–1662, Mar. 2022.

[11] Ng, W.-H., E.-H. Lim, F.-L. Bong, and B.-K. Chung, "E-shaped folded-patch antenna with multiple tuning parameters for on-metal UHF RFID tag," *IEEE Transactions on Antennas and Propagation*, Vol. 67, No. 1, 56–64, Jan. 2019.

[12] Zhang, X., T.-Y. Tan, Q.-S. Wu, L. Zhu, S. Zhong, and T. Yuan, "Pin-loaded patch antenna fed with a dual-mode SIW resonator for bandwidth enhancement and stable high gain," *IEEE Antennas and Wireless Propagation Letters*, Vol. 20, No. 2, 279–283, Feb. 2021.

[13] Qing, X., C. K. Goh, and Z. N. Chen, "Impedance characterization of RFID tag antennas and application in tag co-design," *IEEE Transactions on Microwave Theory and Techniques*, Vol. 57, No. 5, 1268–1274, May 2009.